
NAS-NeRF: Generative Neural Architecture Search for Neural Radiance Fields

Saeejith Nair¹ Yuhan Chen¹ Mohammad Javad Shafiee^{1,2,3} Alexander Wong^{1,2,3}

¹ Vision and Image Processing Research Group, University of Waterloo

² Waterloo Artificial Intelligence Institute, Waterloo, ON

³ DarwinAI Corp., Waterloo, ON

{smnair, yuhan.chen1, mjshafiee, a28wong}@uwaterloo.ca

Abstract

Neural radiance fields (NeRFs) enable high-quality novel view synthesis, but their prohibitively high computational complexity limits deployability, especially on resource-constrained platforms. To enable practical usage of NeRFs, quality tuning is essential to reduce computational complexity, akin to adjustable graphics settings in video games. However while existing solutions strive for efficiency, they use one-size-fits-all architectures regardless of scene complexity, although the same architecture may be unnecessarily large for simple scenes but insufficient for complex ones. Thus as NeRFs become more widely used for 3D visualization, there is a need to dynamically optimize the neural network component of NeRFs to achieve a balance between computational complexity and specific targets for synthesis quality. Addressing this gap, we introduce NAS-NeRF: a generative neural architecture search strategy uniquely tailored to generate NeRF architectures on a per-scene basis by optimizing the trade-off between complexity and performance, while adhering to constraints on computational budget and minimum synthesis quality. Our experiments on the Blender synthetic dataset show the proposed NAS-NeRF can generate architectures up to $5.74 \times$ smaller, with $4.19 \times$ fewer FLOPs, and $1.93 \times$ faster on a GPU than baseline NeRFs, without suffering a drop in SSIM. Furthermore, we illustrate that NAS-NeRF can also achieve architectures up to $23 \times$ smaller, $22 \times$ fewer FLOPs, and $4.7 \times$ faster than baseline NeRFs with only a 5.3% average SSIM drop. The source code for our work is also made publicly available¹.

1 Introduction

Neural radiance fields (NeRFs) enable photorealistic novel view synthesis of complex 3D scenes using limited input imagery. By representing scenes as continuous volumetric radiance and density fields, NeRFs can render high-fidelity views from unseen camera perspectives. A core component in NeRF is the use of multilayer perceptrons (MLPs) to learn a field that models a scene representation function for mapping 5D coordinates (3D location and 2D viewing direction) to volume density and view-dependent emitted radiance.

However, converging to a sufficiently high-resolution representation is computationally demanding, as NeRF requires hundreds of millions of costly neural network queries per rendered image. For example, Mildenhall et al. report that training NeRF [1] on their Blender synthetic dataset requires 640k rays per image, with each ray requiring 256 sampled points that need to be passed through the fields in order to accumulate colour and density. This results in over 150 million network queries per rendered image, which severely limits deployability, especially on resource constrained platforms.

¹Project website: <https://saejjithnair.github.io/NAS-NeRF>

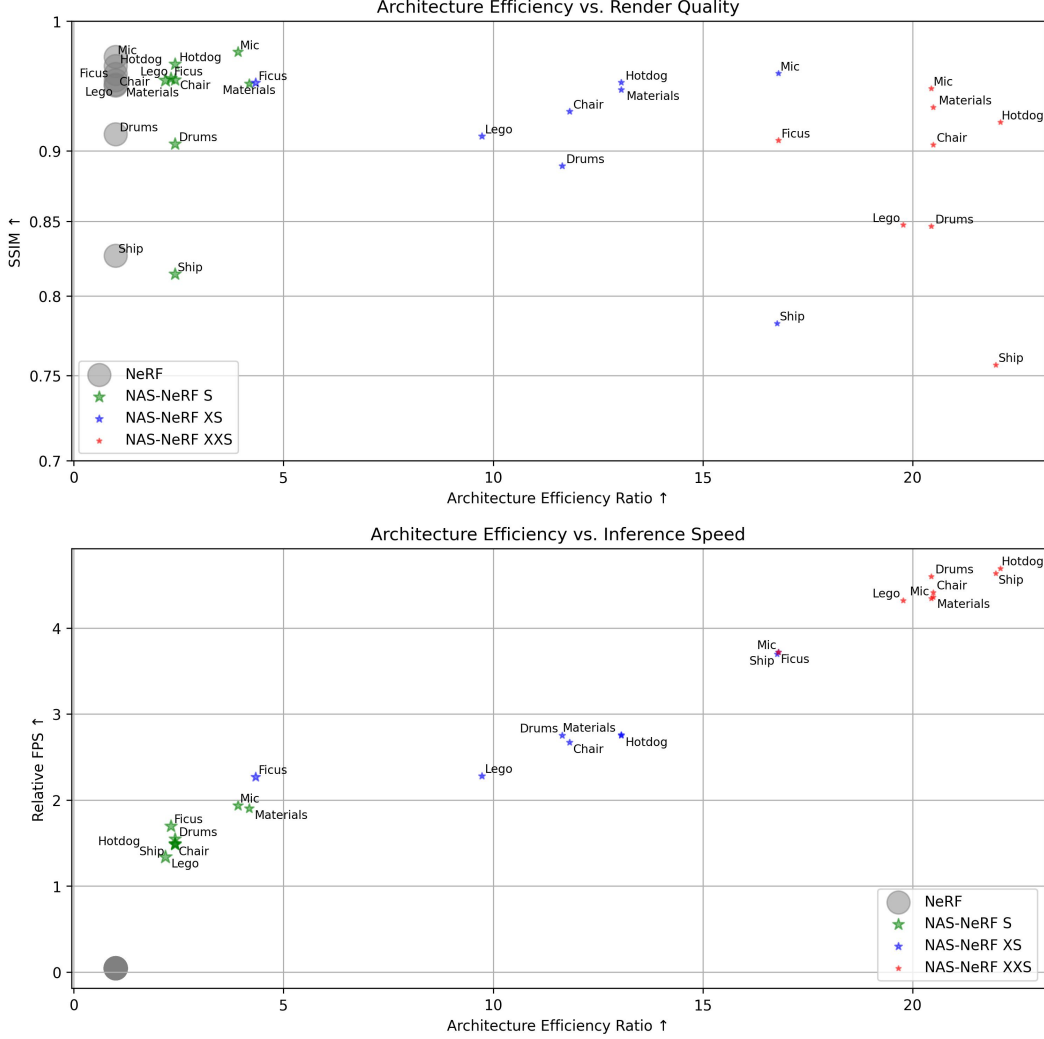


Figure 1: Architecture efficiency ratio vs. synthesis quality (SSIM) (top) and inference speed (bottom), marker size \propto parameter count. Here, architecture efficiency ratio is a measure of the number of FLOPs required for inference on the baseline NeRF architecture relative to the generated NAS-NeRF architecture (see Eq 2) for details.

Although recent advancements have succeeded in enhancing the efficiency of NeRF by employing techniques like caching [2, 3], baking [4], tensor decomposition [5], efficient sampling [6], spatial decomposition [7, 8, 2] or multi-resolution hash encodings [3], these methods maintain the same architectural configuration across various scenes and computational platforms. This one-size-fits-all model neglects the need to balance computational complexity and synthesis quality according to specific deployment constraints. Merely achieving computational efficiency is insufficient if the resulting model compromises the quality of the scene rendering. A more practical design strategy is needed, one that can selectively lower neural network complexity to fit deployment constraints without compromising required synthesis quality. Such a conditional approach permits a more focused exploration of the expansive architectural design space, thereby generating architectures tailored for specific performance criteria.

Our work, NAS-NeRF, executes such a constrained search strategy, and discovers architectures that meet performance constraints while maximizing efficiency. NAS-NeRF leverages a generative synthesis approach [9] to efficiently search the exponential space of all possible NeRF architectures. By incorporating architectural constraints and priors, we guide the search towards promising candidate architecture designs uniquely tailored for a scene. Experiments demonstrate that NAS-NeRF generates

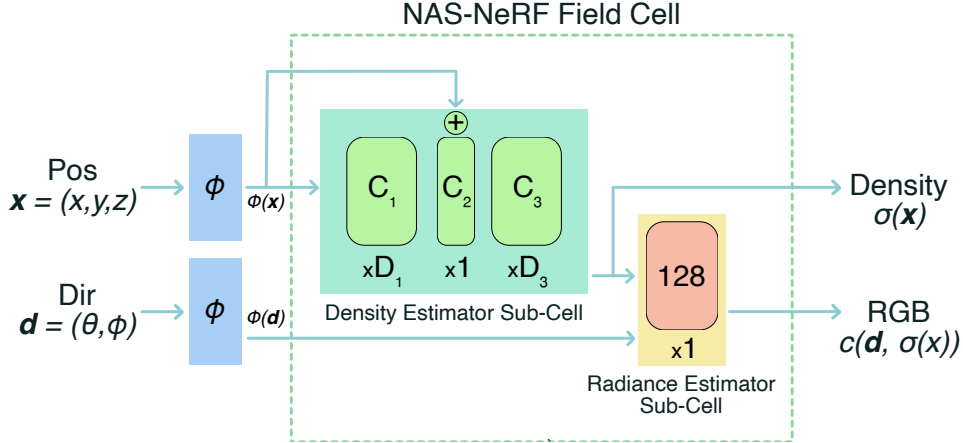


Figure 2: **High level overview of the NAS-NeRF field cell architecture.** The NAS-NeRF pipeline is composed of all the components of the original NeRF [10] pipeline, along with two NAS-NeRF field cells in series for performing the coarse and fine hierarchical sampling. The nature of our parameterization ensures that the NAS-NeRF field cell can be plugged into most other NeRF methods, as our optimizations revolve entirely around the core network architectures.

architectures up to $23\times$ smaller, $22\times$ fewer FLOPs, and $4.7\times$ faster than baseline NeRFs with only a 5.3% average SSIM drop across scenes on the Blender synthetic dataset [1].

The remainder of this paper is organized as follows. Section 2 describes the methodology behind the creation of the proposed NAS-NeRF via generative network architecture search, as well as a description of the resulting NAS-NeRF architectures. Section 3 describes the dataset used in this study, the training and evaluation setup, as well as the experimental results and complexity comparisons.

2 Methods

2.1 NAS-NeRF Field

In this study, we introduce the NAS-NeRF field cell, a generalization of the classic NeRF field introduced in [10], which makes it more amenable to efficient generative network architecture search. The NeRF field represents scenes by learning a continuous 5D function that maps 3D spatial coordinates \mathbf{x} and 2D viewing directions \mathbf{d} to volume density $\sigma(\mathbf{x})$ and view-dependent emitted radiance $c(\mathbf{x}, \mathbf{d})$. These predicted density and radiance values are then used to synthesize RGB images via volumetric rendering techniques.

The NeRF field contains four core components to represent a scene. First, a positional encoding function embeds the input 3D coordinates \mathbf{x} into a higher dimensional space, enabling representation of high-frequency spatial functions. Second, a multilayer perceptron (MLP) with 8 fully-connected layers and 256 channels per layer estimates the volume density value $\sigma(\mathbf{x}) \in [0, 1]$ at each spatial location \mathbf{x} . Third, a viewing direction encoding similarly maps the 2D direction \mathbf{d} to a higher dimensionality. Fourth, a much smaller single layer MLP with 128 channels estimates the radiance (RGB color value) $c(\mathbf{d}, \sigma(\mathbf{x}))$ based on the encoded viewing direction and the predicted density $\sigma(\mathbf{x})$.

Since the large 8-layer density estimator requires modeling the intricate 5D scene function to predict $\sigma(\mathbf{x})$, it contributes most of the trainable parameters in the NeRF field. Thus, we focus our architecture search specifically on optimizing the design of this volume density estimator MLP. As shown in Figure 2, we parameterize the NAS-NeRF density estimator into **three modular stages**, while keeping the smaller radiance estimator fixed:

1. D_1 fully connected layers with C_1 channels
2. $D_2 = 1$ fully connected layer with C_2 channels and a skip connection concatenating the input
3. D_3 fully connected layers with C_3 channels

Decomposing the networks for neural radiance fields into standalone blocks enables reformulating NeRF architecture search as learning specialized cells, with the NeRF field acting analogously to a optimizable cell [11]. Furthermore, this allows viewing the overall NAS-NeRF architecture as two configurable field cells in series - one coarse field cell to learn global structure, and one fine field cell to learn high-frequency details. This modular parametrization focuses optimization on the core NeRF network while decoupling peripheral components like samplers, encoders, and spatial distortions. Our search strategy can thus function as a plugin applied to various NeRF methods by optimizing the architecture of the density estimator sub-cell.

2.2 Generative Network Architecture Search

To discover NAS-NeRF architectures that balance efficiency and novel view synthesis quality, we employ a generative network architecture search approach based on generative synthesis [9]. Given operational constraints like compute budgets and target rendering metrics, generative synthesis executes an architectural exploration process to discover highly tailored architectures fitting the constraints. This discovery process can be formulated as a constrained optimization problem:

$$\mathcal{G} = \max_{\mathcal{G}} \mathcal{U}(\mathcal{G}(s)) \quad \text{subject to} \quad 1_r(G(s)) = 1, \quad \forall s \in \mathcal{S}. \quad (1)$$

where the underlying objective is to learn an expression $\mathcal{G}(\cdot)$ that, given seeds $\{s | s \in S\}$, can generate network architectures $\{N_s | s \in S\}$ that maximizes a universal performance metric U (e.g., [12]) while adhering to operational constraints set by the indicator function $1_r(\cdot)$. This constrained optimization is solved iteratively through a collaboration between a generator G and an inquisitor I which inspects the generated network architectures and guides the generator to improve its generation performance towards operational requirements (see [9] for details).

Although the NAS-NeRF search space is flexible, we enforce design constraints through $1_r(\cdot)$ in Eq. 1 to achieve the desired balance between i) accuracy, ii) architectural complexity, and iii) computational complexity to yield low-footprint, compact NeRF architectures that are tailored for a target performance metric. Specifically, our constraints encourage:

1. Fields with both uniform and variable number of channels across different MLP stages.
2. Fields that uniformly expand such that stages of the MLP get progressively wider.
3. Meeting minimum scene-specific targets T for performance metrics.

In our experiments, we use SSIM [13] as the performance metric and aim to demonstrate discovery of architectures at different scales of efficiency. For each scene, we sample 3 SSIM targets likely to yield models satisfying performance constraints while maximizing compactness. These generated architectures are named NAS-NeRF XXS, XS, and S, with the names mapped based on relative size.

Since NeRF render quality varies per scene, selecting appropriate SSIM targets is crucial. However, determining suitable targets for a new scene leads to a chicken-and-egg dilemma, as we can't know *a priori* what performance can be achieved. To address this circular problem, we propose an efficient heuristic wherein we train two boundary architectures – a maximum size architecture A_{max} and minimum size A_{min} ($> 23.2 \times$ fewer parameters than the baseline) for 16k iterations each (this takes 15-60mins on an NVIDIA RTX A6000 GPU). Using their SSIM evaluations $SSIM_{min}$ and $SSIM_{max}$, we linearly interpolate targets T_{XXS} , T_{XS} , and T_S at 10%, 50%, and 90% between the extremes. Although SSIM versus size may be non-linear along the true pareto frontier, we find that our heuristic provides a reasonable performance bound quickly in a manner that is fast and extensible to any scene or NeRF method. We then leverage the constraints to efficiently discover compact architectures using generative synthesis. By formulating scene-specific SSIM targets and constraining the search, we discover tailored models across a range of complexities specific to each scene's requirements.

2.3 Network Architecture

Table 1 shows the architecture variants generated by NAS-NeRF along with NeRF [10] as the baseline. Compared to NeRF, we can see that for all scenes, the generated NAS-NeRF architectures are much more compact in terms of number of trainable parameters, resulting in up to $4.7 \times$ speedup in terms of frames per second (FPS) when comparing the XXS variants of our architecture with the baseline. While the generated architectures are mostly unique across different scenes, we find that the variants

Scene	Architecture	Coarse Field		Fine Field		FPS	Parameters (M)	FLOPs (G)
	NeRF	Depths	Channels	Depths	Channels	(Speedup)		
	NeRF	8 ×	256	8×	256	1×	1.09 (1×)	574.14 (1×)
Chair	NAS-NeRF S	[2, 1, 1]	[9, 11, 12]	[3, 1, 2]	[200, 207, 214]	1.49×	0.32 (3.46×)	237.57 (2.42×)
Chair	NAS-NeRF XS	[2, 1, 1]	[12, 12, 12]	[3, 1, 2]	[53, 57, 61]	2.67×	0.08 (14.33×)	48.56 (11.82×)
Chair	NAS-NeRF XXS	[2, 1, 1]	[9, 11, 12]	[2, 1, 1]	[16, 18, 20]	4.41×	0.05 (21.92×)	28.01 (20.49×)
Drums	NAS-NeRF S	[2, 1, 1]	[9, 11, 12]	[3, 1, 2]	[200, 207, 214]	1.55×	0.32 (3.46×)	237.57 (2.42×)
Drums	NAS-NeRF XS	[2, 1, 1]	[20, 20, 20]	[3, 1, 2]	[53, 57, 61]	2.75×	0.08 (13.81×)	49.29 (11.65×)
Drums	NAS-NeRF XXS	[2, 1, 1]	[12, 12, 12]	[2, 1, 1]	[16, 18, 20]	4.60×	0.05 (21.82×)	28.08 (20.45×)
Ficus	NAS-NeRF S	[2, 1, 1]	[12, 12, 12]	[3, 1, 2]	[214, 214, 214]	1.70×	0.33 (3.32×)	247.57 (2.32×)
Ficus	NAS-NeRF XS	[2, 1, 1]	[9, 11, 12]	[2, 1, 1]	[167, 174, 180]	2.27×	0.18 (5.99×)	132.33 (4.34×)
Ficus	NAS-NeRF XXS	[2, 1, 1]	[9, 11, 12]	[2, 1, 1]	[33, 36, 39]	3.72×	0.06 (18.94×)	34.17 (16.80×)
Hotdog	NAS-NeRF S	[2, 1, 1]	[9, 11, 12]	[3, 1, 2]	[200, 207, 214]	1.49×	0.32 (3.46×)	237.57 (2.42×)
Hotdog	NAS-NeRF XS	[2, 1, 1]	[12, 12, 12]	[3, 1, 2]	[51, 51, 51]	2.75×	0.07 (15.51×)	43.98 (13.05×)
Hotdog	NAS-NeRF XXS	[2, 1, 1]	[12, 12, 12]	[2, 1, 1]	[9, 11, 12]	4.69×	0.05 (23.05×)	25.98 (22.10×)
Lego	NAS-NeRF S	[2, 1, 1]	[100, 104, 109]	[3, 1, 2]	[214, 214, 214]	1.34×	0.39 (2.83×)	262.61 (2.19×)
Lego	NAS-NeRF XS	[2, 1, 1]	[12, 12, 12]	[4, 1, 3]	[64, 64, 64]	2.28×	0.09 (12.19×)	58.98 (9.73×)
Lego	NAS-NeRF XXS	[2, 1, 1]	[16, 18, 20]	[2, 1, 1]	[20, 20, 20]	4.32×	0.05 (20.64×)	29.03 (19.78×)
Materials	NAS-NeRF S	[2, 1, 1]	[16, 18, 20]	[2, 1, 1]	[180, 180, 180]	1.90×	0.19 (5.74×)	137.17 (4.19×)
Materials	NAS-NeRF XS	[2, 1, 1]	[12, 12, 12]	[3, 1, 2]	[51, 51, 51]	2.76×	0.07 (15.51×)	43.98 (13.05×)
Materials	NAS-NeRF XXS	[2, 1, 1]	[9, 11, 12]	[2, 1, 1]	[16, 18, 20]	4.36×	0.05 (21.92×)	28.01 (20.49×)
Mic	NAS-NeRF S	[4, 1, 3]	[56, 60, 64]	[2, 1, 1]	[180, 180, 180]	1.93×	0.23 (4.83×)	146.53 (3.92×)
Mic	NAS-NeRF XS	[2, 1, 1]	[9, 11, 12]	[2, 1, 1]	[33, 36, 39]	3.72×	0.06 (18.94×)	34.17 (16.80×)
Mic	NAS-NeRF XXS	[2, 1, 1]	[12, 12, 12]	[2, 1, 1]	[16, 18, 20]	4.34×	0.05 (21.82×)	28.08 (20.45×)
Ship	NAS-NeRF S	[2, 1, 1]	[9, 11, 12]	[3, 1, 2]	[200, 207, 214]	1.48×	0.32 (3.46×)	237.57 (2.42×)
Ship	NAS-NeRF XS	[2, 1, 1]	[12, 12, 12]	[2, 1, 1]	[33, 36, 39]	3.69×	0.06 (18.86×)	34.23 (16.77×)
Ship	NAS-NeRF XXS	[2, 1, 1]	[9, 11, 12]	[2, 1, 1]	[12, 12, 12]	4.63×	0.05 (23.05×)	26.11 (21.99×)

Table 1: **The architecture configuration and performance metrics of each generated NAS-NeRF is shown, along with the baseline NeRF [10].** The architecture configurations for GEN-NeRF are listed as $[D_1, D_2, D_3]$ for the depth columns and $[C_1, C_2, C_3]$ for the channels columns. The architecture configuration for the baseline NeRF model is also listed as each field has an MLP with 8 layers and 256 channels. The FPS and Parameters columns show the frames per second and the number of parameters of each model, along with the speedup and architecture efficiency ratio relative to the baseline NeRF architecture.

still have relatively consistent characteristics across scenes, owing to the way in how the performance target was specified. For example compared to the baseline NeRF architecture’s computational complexity (FLOPs), the S variants are 2.19-4.19× more efficient, XS variants are 4.34-16.8× more efficient, and the XXS variants are 16.8-22.1× more efficient. Surprisingly, we find that in certain instances, the same architecture was generated multiple times but for different scales of the target performance metric on separate scenes. For example, the same architecture was generated for both the Ficus scene and the Mic scene, except at the XXS scale for the former and XS scale for the latter.

Another interesting finding is that there is lots of similarity in the coarse field architecture between NAS-NeRF variants across scenes, with most of the generated architectures converging to an extremely tiny field representation. This supports both prior work [14] and intuition which suggests that the fine field is more important than the coarse field, as most of the key features in a scene are embedded in the high frequency details.

While the generated coarse field architectures have some degree of homogeneity, we find that this is not at all the case for the fine field architectures. While the network depths for each generated stage are relatively consistent across different scenes, there is a lot more diversity to the widths of each stage, across both NAS-NeRF variants and scenes. Specifically, while most coarse field architectures had stages with uniform widths, we find that many more of the fine field architecture stages have widths with variable but uniformly increasing number of channels.



Figure 3: **Qualitative results of each of our NAS-NeRF architectures evaluated on the corresponding scene it was generated for, along with the ground truth image and NeRF baseline.** Red box shows a magnified view of an image patch.

PSNR \uparrow										
Architecture	Chair	Drums	Ficus	Hotdog	Lego	Materials	Mic	Ship	Mean	
NeRF	31.259	24.607	29.086	34.137	31.319	29.428	31.089	27.669	29.824	
NAS-NeRF S	31.205	24.129	28.382	34.312	31.720	29.526	31.711	26.985	29.746	
NAS-NeRF XS	29.423	23.215	28.100	32.307	28.266	29.135	29.313	24.876	28.079	
NAS-NeRF XXS	27.756	20.849	24.526	28.921	25.047	27.627	27.887	22.525	25.642	
SSIM \uparrow										
Architecture	Chair	Drums	Ficus	Hotdog	Lego	Materials	Mic	Ship	Mean	
NeRF	0.953	0.912	0.958	0.964	0.950	0.949	0.971	0.827	0.936	
NAS-NeRF S	0.953	0.905	0.954	0.966	0.953	0.950	0.975	0.814	0.934	
NAS-NeRF XS	0.929	0.889	0.951	0.951	0.911	0.946	0.958	0.782	0.915	
NAS-NeRF XXS	0.904	0.847	0.908	0.921	0.848	0.932	0.947	0.757	0.883	
LPIPS \downarrow										
Architecture	Chair	Drums	Ficus	Hotdog	Lego	Materials	Mic	Ship	Mean	
NeRF	0.043	0.089	0.039	0.039	0.027	0.042	0.033	0.179	0.061	
NAS-NeRF S	0.041	0.100	0.045	0.035	0.026	0.038	0.025	0.191	0.063	
NAS-NeRF XS	0.071	0.124	0.046	0.062	0.057	0.044	0.052	0.266	0.090	
NAS-NeRF XXS	0.110	0.213	0.086	0.127	0.131	0.061	0.076	0.320	0.141	

Table 2: **Per-scene quantitative results on the Blender synthetic dataset comparing the generated architectures with the baseline NeRF model.** The last column shows the mean performance metric score for each architecture averaged across all scenes.

3 Experiments

We evaluate the SSIM [13], PSNR, and LPIPS [15] of our generated architectures on its corresponding scene from the Blender Synthetic dataset [10] and compare against the original NeRF [10] architecture as our baseline. To ensure that all architectures are trained to a comparable level, we scale the number of training iterations proportional to the architecture parameters efficiency ratio ER_{params} and relative to the number of training iterations required for the baseline NeRF architecture (200k iterations). The architecture efficiency ratio ER is defined as follows and the metric used for this situation is parameter count.

$$ER = \frac{\text{Baseline Architecture Metric}}{\text{Generated Architecture Metric}} \quad (2)$$

We develop all our code leveraging the Nerfstudio framework [16] in order to maximize reproducibility and extensibility, and open source our repo². All architectures are trained using the default hyperparameters for the Vanilla NeRF model in Nerfstudio v0.2.1 (i.e. RAdam optimizer with a learning rate of 5×10^{-4}).

As seen in Table 2, our generated architectures are quite competitive considering their size, with the NAS-NeRF S variants either out-performing or being comparable to the baseline NeRF architecture despite being $2\text{-}4\times$ smaller and up to $1.93\times$ faster. The NAS-NeRF XXS variants also achieve SSIM performance metrics that are only a 5.3% drop on each scene compared to the baseline NeRF, while being more than $23\times$ smaller and up to $4.7\times$ faster. Qualitative visual comparisons of our generated architectures against the ground truth scene and NeRF representation show that both the NAS-NeRF S

²<https://saeejithnair.github.io/NAS-NeRF/>

and NAS-NeRF XS variants appear to achieve rendering quality that is competitive with the baseline NeRF architecture. While the quantitative results from the NAS-NeRF XXS variants are encouraging, visual comparison indicates that the smallest models may not have enough capacity to learn all the high frequency details necessary for robust novel view synthesis. Nonetheless, we believe that this limitation can be overcome by pairing our generative architecture strategy with newer NeRF methods which leverage more robust strategies around geometric encoding, sampling, spatial distortion, and hierarchical scene representation.

4 Conclusion

Our work introduces NAS-NeRF, a family of NeRF architectures that are tailored per scene and compute budget. By executing a generative neural architecture search strategy, we show that our method can discover architectures at varying scales of efficiency (NAS-NeRF XXS, XS, and S), thus introducing a way for developers and researchers to systematically make trade offs between performance target quality and architecture complexity, while still remaining at the pareto frontier. By developing NeRF models that achieve competitive performance with baseline NeRF architectures while being a fraction of the size, we hope to open the door to enabling more widespread deployment of novel view synthesis techniques on resource constrained devices like mobile phones and embedded systems.

References

- [1] Ben Mildenhall, Pratul P. Srinivasan, Matthew Tancik, Jonathan T. Barron, Ravi Ramamoorthi, and Ren Ng. Nerf: Representing scenes as neural radiance fields for view synthesis. In *ECCV*, 2020.
- [2] Stephan J. Garbin, Marek Kowalski, Matthew Johnson, Jamie Shotton, and Julien Valentin. FastNeRF: High-fidelity neural rendering at 200fps. pages 14346–14355. URL https://openaccess.thecvf.com/content/ICCV2021/html/Garbin_FastNeRF_High-Fidelity_Neural_Rendering_at_200FPS_ICCV_2021_paper.html.
- [3] Thomas Müller, Alex Evans, Christoph Schied, and Alexander Keller. Instant neural graphics primitives with a multiresolution hash encoding. 41(4):1–15. ISSN 0730-0301, 1557-7368. doi: 10.1145/3528223.3530127. URL <https://dl.acm.org/doi/10.1145/3528223.3530127>.
- [4] Peter Hedman, Pratul P. Srinivasan, Ben Mildenhall, Jonathan T. Barron, and Paul Debevec. Baking neural radiance fields for real-time view synthesis. pages 5875–5884. URL https://openaccess.thecvf.com/content/ICCV2021/html/Hedman_Baking_Neural_Radiance_Fields_for_Real-Time_View_Synthesis_ICCV_2021_paper.html.
- [5] Anpei Chen, Zexiang Xu, Andreas Geiger, Jingyi Yu, and Hao Su. TensoRF: Tensorial radiance fields. In Shai Avidan, Gabriel Brostow, Moustapha Cissé, Giovanni Maria Farinella, and Tal Hassner, editors, *Computer Vision – ECCV 2022*, Lecture Notes in Computer Science, pages 333–350. Springer Nature Switzerland. ISBN 978-3-031-19824-3. doi: 10.1007/978-3-031-19824-3_20.
- [6] T. Neff, P. Stadlbauer, M. Parger, A. Kurz, J. H. Mueller, C. R. A. Chaitanya, A. Kapanyan, and M. Steinberger. DONeRF: Towards real-time rendering of compact neural radiance fields using depth oracle networks. 40(4):45–59. ISSN 1467-8659. doi: 10.1111/cgf.14340. URL <https://onlinelibrary.wiley.com/doi/abs/10.1111/cgf.14340>. _eprint: <https://onlinelibrary.wiley.com/doi/pdf/10.1111/cgf.14340>.
- [7] Daniel Rebain, Wei Jiang, Soroosh Yazdani, Ke Li, Kwang Moo Yi, and Andrea Tagliasacchi. DeRF: Decomposed radiance fields. pages 14153–14161. URL https://openaccess.thecvf.com/content/CVPR2021/html/Rebain_DeRF_Decomposed_Radiance_Fields_CVPR_2021_paper.html.
- [8] Christian Reiser, Songyou Peng, Yiyi Liao, and Andreas Geiger. KiloNeRF: Speeding up neural radiance fields with thousands of tiny MLPs. pages 14335–14345. URL https://openaccess.thecvf.com/content/ICCV2021/html/Reiser_KiloNeRF_Speeding_Up_Neural_Radiance_Fields_With_Thousands_of_Tiny_ICCV_2021_paper.html.
- [9] Alexander Wong, Mohammad Javad Shafiee, Brendan Chwyl, and Francis Li. FermiNets: Learning generative machines to generate efficient neural networks via generative synthesis. URL <http://arxiv.org/abs/1809.05989>.

- [10] Ben Mildenhall, Pratul P. Srinivasan, Matthew Tancik, Jonathan T. Barron, Ravi Ramamoorthi, and Ren Ng. NeRF: Representing scenes as neural radiance fields for view synthesis. In Andrea Vedaldi, Horst Bischof, Thomas Brox, and Jan-Michael Frahm, editors, *Computer Vision – ECCV 2020*, Lecture Notes in Computer Science, pages 405–421. Springer International Publishing. ISBN 978-3-030-58452-8. doi: 10.1007/978-3-030-58452-8_24.
- [11] Barret Zoph and Quoc V. Le. Neural architecture search with reinforcement learning. URL <http://arxiv.org/abs/1611.01578>.
- [12] Alexander Wong. NetScore: Towards universal metrics for large-scale performance analysis of deep neural networks for practical on-device edge usage. In Fakhri Karray, Aurélio Campilho, and Alfred Yu, editors, *Image Analysis and Recognition*, Lecture Notes in Computer Science, pages 15–26. Springer International Publishing. ISBN 978-3-030-27272-2. doi: 10.1007/978-3-030-27272-2_2.
- [13] Zhou Wang, A.C. Bovik, H.R. Sheikh, and E.P. Simoncelli. Image quality assessment: from error visibility to structural similarity. 13(4):600–612. ISSN 1941-0042. doi: 10.1109/TIP.2003.819861. Conference Name: IEEE Transactions on Image Processing.
- [14] Tao Hu, Shu Liu, Yilun Chen, Tiancheng Shen, and Jiaya Jia. EfficientNeRF efficient neural radiance fields. pages 12902–12911. URL https://openaccess.thecvf.com/content/CVPR2022/html/Hu_EfficientNeRF_Efficient_Neural_Radiance_Fields_CVPR_2022_paper.html.
- [15] Richard Zhang, Phillip Isola, Alexei A. Efros, Eli Shechtman, and Oliver Wang. The unreasonable effectiveness of deep features as a perceptual metric. pages 586–595. URL https://openaccess.thecvf.com/content_cvpr_2018/html/Zhang_The_Unreasonable_Effectiveness_CVPR_2018_paper.html.
- [16] Matthew Tancik, Ethan Weber, Evonne Ng, Ruilong Li, Brent Yi, Justin Kerr, Terrance Wang, Alexander Kristoffersen, Jake Austin, Kamyar Salahi, Abhik Ahuja, David McAllister, and Angjoo Kanazawa. Nerfstudio: A modular framework for neural radiance field development. In *Special Interest Group on Computer Graphics and Interactive Techniques Conference Conference Proceedings*, pages 1–12. doi: 10.1145/3588432.3591516. URL <http://arxiv.org/abs/2302.04264>.